A novel laminar kinetic energy model for the prediction of pretransitional velocity fluctuations and boundary layer transition

Medina, H, Beechook, A, Fadhila, HN, Aleksandrova, S & Benjamin, S

Original citation & hyperlink:
Medina, H, Beechook, A, Fadhila, HN, Aleksandrova, S & Benjamin, S 2018, 'A novel laminar kinetic energy model for the prediction of pretransitional velocity fluctuations and boundary layer transition' *International Journal of Heat and Fluid Flow*, vol 69, pp. 150-163
https://dx.doi.org/10.1016/j.ijheatfluidflow.2017.12.008

DOI 10.1016/j.ijheatfluidflow.2017.12.008
ISSN 0142-727X

Publisher: Elsevier

A novel laminar kinetic energy model for the prediction of pretransitional velocity fluctuations and boundary layer transition

H. Medina[a,*], A. Beechook[a], H. Fadhila[a], S. Aleksandrova[a], S. Benjamin[a]

[a] *Coventry University, Centre for Mobility and Transport, Coventry, United Kingdom*

Abstract

Boundary layer transition onset estimation and modelling are essential for the design of many engineering products across many industries. In this work, a novel model for predicting pretransitional boundary layer fluctuations is proposed. The laminar kinetic energy (LKE) concept is used to represent such fluctuations. The new LKE model is implemented in OpenFOAM within the Reynolds-Averaged Navier-Stokes (RANS) framework. Only two approaches for modelling the LKE can be found in the literature. Mayle and Schulz aproach (1997) has the limitation of requiring an initial LKE profile. Walter and Cokljat's (2008) approach has been found to significantly overpredict the growth of the LKE. In addition, their model is tightly coupled with the specific dissipation rate and turbulent kinetic energy equations. The new model proposed here can act as a stand-alone equation for the LKE, making it portable and potentially facilitating the development of new transition models tailored to various industrial applications. Comparison with experiments shows that the new LKE model correctly predicts the growth of pretransitional velocity fluctuations and skin friction for a flat plate at zero-pressure gradient. To illustrate its practical application for transitional flows, the LKE model is coupled with an existing $k-\omega$ model using a new approach that requires minimal modifications. The resulting model ($k-\omega$ LKE) demonstrates excellent predictive capabilities when applied to a number of validation test cases.

Keywords: Laminar kinetic energy, boundary layer, transition, OpenFOAM, plate,, separation, bubble

1. Introduction

The principal focus of the subject of boundary layer transition modelling is to develop and use models that can predict the extent of the laminar, transitional and turbulent regions that may appear in a given application and system configuration. The ability to accurately predict the breakdown to turbulence is essential to engineers in many engineering applications. Specific examples include: aircraft drag estimation and fuel consumption, turbine blades, pressure losses in automotive emission reduction systems, etc.

When the freestream turbulence intensity is low, disturbances within the boundary layer predominantly grow in the form of Tollmien-Schlichting waves (although other modes may also arise [1, 2]) until they eventually amplify to the point when they breakdown into turbulence. This process is known as natural transition. In natural transition, the growth of disturbances can be described by the primary modes of the Orr-Sommerfeld equation. The e^N method [3–5], which is popular within the aerospace industry, examines the amplification rate of the most unstable Tollmien-Schilchting wave along a surface and transition onset is assumed once a given N-factor is reached. Whilst the e^N has been widely successful, it is difficult to extend to complex geometries or implement into general Computational Fluid Dynamics (CFD) codes. On the other hand, bypass transition occurs as the freestream turbulence intensity is increased and Tollmien-Schilchting waves no longer develop and are altogether bypassed (intermediate paths exist, see e.g. [2]). Under these conditions, the e^N method is no longer suitable and, traditionally, correlation based methods have been employed [6, 7]. More recently, boundary layer transition has also been investigated using high-fidelity simulation techniques such as Direct Numerical Simulation (DNS) and Large Eddy Simulation (LES) [8–12]. Despite growing computing power, their computational cost is too restrictive for day-to-day industrial applications [13, 14]. Consequently, the Reynolds-Averaged Navier Stokes (RANS) approach for modelling transitional flows continues to be an area of interest because RANS-based modelling offers a reasonable compromise between computational expense and accuracy. For this reason and due to the potential engineering applications of this work a RANS-based approach has been adopted here.

Progress on the development of transition sensitive RANS models has been steady. An examination of the literature on recent RANS models developed to predict boundary layer transition shows that there are two main approaches: (i) to couple turbulent models with empirical correlations and (ii) to extend turbulence models by including additional transport equations to model transitional behaviour. The first approach involves the incorporation of suitable experimental

*Corresponding author
Email address: h.medina@coventry.ac.uk (H. Medina)
URL: www.aerofluids.org (H. Medina)

Nomenclature

Acronyms

CFD	Computational fluid dynamics	
DNS	Direct numerical simulation	
LES	Large eddy simulation	
LKE	Laminar kinetic Energy	
$RANS$	Reynolds-Averaged Navier Stokes	
ZPG	Zero pressure gradient	

Greek Symbols

α_L	Laminar diffusion eddy viscosity	$[m^2/s]$
ϵ	Dissipation rate	$[m^2/s^3]$
η	Laminar production coefficient	
γ	Transition initiation function	
Λ	Integral length scale	$[m]$
ν	Laminar kinetic viscosity	$[m^2/s]$
ν_L	Laminar kinetic eddy viscosity	$[m^2/s]$
ν_R	Eddy viscosity ratio: ν_t/ν	
ν_t	Turbulent kinetic eddy viscosity	$[m^2/s]$
$\nu_{t,s}$	Small-scale eddy viscosity	$[m^2/s]$
Ω	Magnitude of shear rate tensor: $\sqrt{2\Omega_{ij}\Omega_{ij}}$	$[s^{-1}]$
ω	Specific dissipation rate	$[s^{-1}]$
ω_d	Frequency driving LKE growth	$[s^{-1}]$
ρ	Fluid density	$[kg/m^3]$
τ_η	Komogorov's time scale	$[s]$
τ_w	Wall shear stress: $\mu\left(\frac{\partial U}{\partial y}\right)_{y=0}$	$[N/m^2]$
υ	Kolmogorov's velocity scale	$[m/s]$
ξ	Convective frequency: $\xi = S$	$[s^{-1}]$

Roman Symbols

C_P'	Modified pressure coefficient	
C_P	Pressure coefficient	
f_v	Viscous damping function	
f_{SS}	Shear-sheltering damping function	
k	Turbulent kinetic energy	$[m^2/s^2]$
k_L	Laminar kinetic energy	$[m^2/s^2]$
P	Mean pressure	$[Pa]$
p'	Fluctuating pressure	$[Pa]$
P_{k_L}	Production of k_L	$[m^2/s^3]$
Re	Reynolds number: $\frac{U_\infty L}{\nu}$	
Re_Λ	Integral Reynolds number: $\frac{U_\infty \Lambda}{\nu}$	
S	Magnitude of strain rate tensor: $\sqrt{2S_{ij}S_{ij}}$	$[s^{-1}]$
S_{ij}	Strain rate tensor: $\frac{1}{2}\left(\frac{\partial U_i}{\partial x_j} + \frac{\partial U_j}{\partial x_i}\right)$	$[s^{-1}]$
t	Time	$[s]$
t_Λ	Integral time scale	$[s]$
Tu	Turbulence intensity: u'_{rms}/U_∞	
U	Mean velocity	$[m/s]$
u'	Streamwise fluctuating velocity	$[m/s]$
u_i	Velocity vector	$[m/s]$
v'	Wall-normal fluctuating velocity	$[m/s]$
x	Streamwise coordinate	$[m]$
y	Wall-normal distance	$[m]$
y^+	Dimensionless wall-normal distance	

Subscripts

∞	Refers to freestream condition
eff	Refers to effective
$inlet$	Refers to inlet condition or value
L	Refers to laminar
max	Refers to maximum condition
min	Refers to minimum condition
rms	Root-mean squared of quantity
SS	Refers to shear-sheltering effects
T	Refers to turbulent
$wall$	Refers to wall or near-wall conditions

transition correlations [6, 7] which are used to control transition initiation. The difficulty of using this approach is that experimental correlations often require non-local variables such as the momentum thickness or displacement thickness which makes them challenging to implement into CFD packages. Additionally, models based on empirical correlations may not be universal since their range of applicability is limited to how closely the intended application operating conditions match those of the experiments from which the correlations were derived in the first place. The second approach involves the development of more general transition sensitive models by incorporating additional transport equations. For instance, Suzen and Huang [15] used an equation for intermittency to control transition onset. The approach of using auxiliary equations to complement turbulence models has also been successfully demonstrated by Steelant and Dick

[16] and Menter et al. [17, 18]. Since experimental correlations are embedded into these models, their predictive capabilities are limited. An alternative method is to develop phenomenological models or physics-based models [19–22].

The development of phenomenological transitional models is certainly desirable since they attempt to incorporate the physics of boundary layer transition directly. Nonetheless, this is a very challenging endeavour particularly due the fact that many of the mechanisms influencing boundary layer transition are not yet fully understood e.g. receptivity mechanisms to external disturbances or 3-dimensional effects due to pressure gradients of complex geometries. However, Walters and Cokljat [22] developed a three equation phenomenological transition model ($k - k_L - \omega$) based on the concept of the laminar kinetic energy, first proposed by Mayle and Schulz [23]. The $k - k_L - \omega$ model has the advantage of using local variables to predict the onset of transition. Also, thanks to its ease of implementation the $k - k_L - \omega$ is available in commercial and open source CFD packages. Furthermore, Medina and Early [24] demonstrated the flexibility of the laminar kinetic framework by proposing a simple modification to enable the prediction of boundary layer transition due to aft-facing steps. Recently, Qin et al. [25] showed that the laminar kinetic framework used by the $k - k_L - \omega$ can also be extended to accommodate hypersonic flow. Despite the many advantages of the $k - k_L - \omega$ model, there is evidence in the literature [26, 27] that this model, whilst capable of predicting the linear portion of the lift curve (lift coefficient versus angle of attack), it tends to fail in capturing stall on aerofoils and overpredicts lift generation. In an attempt to identify the reason for this behaviour the authors of this work realised that the $k - k_L - \omega$ model can drastically over predict the laminar kinetic energy and consequently the relative influence of streamwise fluctuations within the boundary layer (as it will be shown later). This realisation provided the motivation for this work. Furthermore, the laminar kinetic energy (LKE) equation used in the $k - k_L - \omega$ model uses the specific dissipation rate, ω, and the turbulent kinetic energy, k, as auxiliary variables. As a result, it can not be used as a stand-alone model which makes it difficult to adapt or use in conjunction with other turbulence models. In this work, a novel model for the LKE is proposed which has been developed by revisiting the work of Mayle and Schulz [23] with the aim of producing a stand-alone LKE model equation which only requires the calculated mean velocity field and an effective turbulence level as user input. To illustrate how the new LKE model can be used for transitional flows of practical interest, the model is coupled with a version of Wilcox's $k - \omega$ model [28] using a new approach inspired on the work of Kubacki and Dick [29, 30]. The resulting model ($k - \omega$ LKE) is validated using a number of test cases involving transitional flows.

2. New LKE model development

2.1. Background

For freestream turbulence intensities below approximately 1% low amplitude pretransitional velocity fluctuations typically appear as two-dimensional travelling waves known as Tollmien-Schlichting waves [31] and the average pretransitional velocity profile is essentially laminar. For higher freestream turbulence intensities, the mean velocity profile can deviate from the Blasius velocity profile and relatively high amplitude streamwise velocity fluctuations are generated. These fluctuations eventually break down leading to a turbulent boundary layer. This process is known as bypass transition.

In bypass transition, the pretransitional velocity fluctuations are regarded as Klebanoff modes [32] and are not considered as turbulence. Mayle and Schulz [23] exploited this distinction for modelling purposes and proposed the concept of the laminar kinetic energy (LKE) to describe the development of these pretransitional velocity fluctuations which lead to bypass transition. They define the laminar kinetic energy as the energy due to the pretransitional velocity fluctuations, i.e. $k_L = \overline{u'}^2/2$, and by extending Lin's work [33], developed a new transport equation for the LKE as shown in equation 1.

$$\overline{U}\frac{\partial k_L}{\partial x} + \overline{V}\frac{\partial k_L}{\partial y} = -(\overline{u'v'})\frac{\partial \overline{u}}{\partial y} - \frac{\partial}{\partial y}\left(\overline{v'}k_L - \nu\frac{\partial k_L}{\partial y}\right) - \epsilon + \left(\overline{u'\frac{\partial U'}{\partial t}}\right) \tag{1}$$

Following an analysis to estimate the relative orders of magnitudes for the various terms of equation 1, Mayle and Schulz [23] conclude that only the last term in equation 1 can become sufficiently large to overcome dissipation and drive the production of laminar kinetic energy. This term is derived by taking the average of the pressure diffusion term in the kinetic energy budget ($u'(\partial p'/\partial x)$) and it drives the production of LKE by freestream pressure fluctuations. Mayle and Schulz [23] propose that this term can be modelled as $\omega_{eff}\sqrt{kk_{eff}}$, where ω_{eff} and k_{eff} represent an effective driving frequency and kinetic energy, respectively. Ultimately, they propose a model for the production term in the LKE equation as shown in equation 2. The effective kinetic energy is replaced by the incoming freestream value and the driving frequency is assumed to be proportional to the ratio between the square of the freestream velocity and the laminar kinematic viscosity. However, the ratio U_∞^2/ν is not truly representative of the actual forcing frequency and only serves to provide dimensional consistency.

$$\overline{u'\frac{\partial U'}{\partial t}} = C_\omega \frac{U_\infty^2}{\nu}\sqrt{k_L k_\infty}\, e^{-y^+/c^+} \tag{2}$$

In order to provide a link between the freestream turbulence characteristics and the growth or production of LKE, Mayle and Schulz [23] also proposed to include a functional constant C_ω. Following a rather elegant analysis (details not included here for succinctness - interested readers are referred to [23]), they propose an extended production term as shown in equation 3.

$$\overline{u'\frac{\partial U'}{\partial t}} = C\left(\frac{\upsilon}{U_\infty}\right)^{2/3} Re_\Lambda^{-1/3}\frac{U_\infty^2}{\nu}\sqrt{k_L k_\infty}\, e^{-y^+/c^+} \tag{3}$$

In their analysis Mayle and Schulz [23] also show that the LKE grows as $\sqrt{k_L} = \sqrt{k_{L_\infty}(\omega_d x/U_\infty)}$. Remarkably, following this approach, and provided sufficient information is available about the freestream turbulence spectrum, Mayle and Schulz [23] show that the coefficient C effectively collapses to a value around 0.07. A key finding from their work is the notion that the growth of LKE is linked to both the Kolmogorov's velocity scale, υ, and the integral Reynolds number, Re_Λ. In the new LKE model proposed in this work, this finding is exploited as a means to scale (and almost linearise) the production of LKE in relation to the upstream turbulence intensity.

Mayle's model has some weaknesses, for example, sufficient information about the turbulence spectrum is necessary in order to estimate Re_Λ and υ. Additionally, the model also requires the definition of the LKE profile at the inlet boundary. These weaknesses make the model difficult to apply for general purpose CFD transition models on more complex geometries. Since it is a stand-alone model equation, it can be integrated into a turbulence model to enable the prediction of boundary layer transition [34]. Walters et al. [20–22] have proposed a pioneering alternative approach to modelling the LKE which resolves the need to provide an initial profile. They assumed that the production of LKE is a result of the interaction of the Reynolds stresses due to pretransitional velocity fluctuations and the mean shear. That is, changes to the pretransitional mean velocity profile are due to a loss of mean flow kinetic energy. This is also confirmed in [35]. This suggests that the commonly used strain-based production approach is justified. Therefore, a similar mechanism to drive the production of LKE is also employed in this work.

A disadvantage of the LKE model proposed by Walters et al. [20–22] is that the LKE energy equation (and production term) is coupled with the turbulent kinetic energy and the dissipation rate equations [20, 21] (or specific dissipation rate [22]). Additionally, a closer assessment of the more popular model proposed by Walters and Cokljat [22], the well-known $k-k_L-\omega$ model, reveals that it can drastically overpredict the growth of LKE as shown in figure 1. This weakness also provided the motivation to develop a new LKE model.

2.2. New approach and concepts

The requirements for the new model include the ability to reproduce the accuracy of the model proposed by Mayle and Schulz [23] and retain the ease of use and generality of the $k-k_L-\omega$ model [22]. In order to meet these requirements,

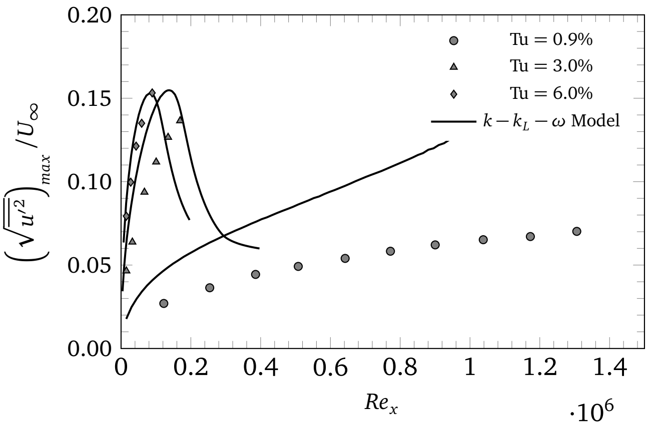

Figure 1: Maximum value of the streamwise velocity fluctuations predicted by the $k-k_L-\omega$ model compared with ERCOFTAC's ZPG cases [36]

a new production term (6 in section 2.3) is proposed. In the work of Mayle and Shulz [7], the underlying model for the growth of LKE is $\omega_{eff}\sqrt{k_L k_{eff}}$. In the present work it has been based on the classical strain-based production mechanism, similar to the approach of Walters et al. [20–22]. That is, production is mainly driven by the product of the LKE and the strain rate, $k_L S$, which essentially replaces the effective frequency, ω_{eff}, by the convection frequency scale $\xi = S$. However, this expression does not scale correctly and a new approach to scaling the production of the LKE is needed.

As introduced previously, Mayle ans Schulz [23] scale their model using the integral Reynolds number, Re_Λ, and the Kolmogorov's velocity scale, calculated from the freestream turbulence spectrum. Unfortunately, this information is not always available. To generalise the approach, here, instead of utilising the freestream turbulence spectrum, it is suggested that scaling can be achieved by incorporating functional forms into the model. Two functions are defined for this purpose: an integral scale Reynolds number (Re_Λ, equation 8) and a Reynolds number based on Kolmogorov's velocity scale (Re_υ, equation 7). Next, their relative influence on LKE production remains to be determined.

In equation 2, it can be observed that the production term to be modelled has the form of a forcing function in time (i.e $\propto \overline{\partial U'/\partial t}$) dominated by the large scales. Therefore, it is proposed to scale temporal effects using the ratio of the integral to Kolmogorov's time scales i.e. t_Λ/τ_η. The integral time can be determined from the integral velocity and time scales, such that $t_\Lambda = \Lambda/U$. The Kolmogorov time scale can be approximated as $\tau_\eta = (\nu/\epsilon)^{1/2}$. At the smallest scales supply and dissipation of kinetic energy are equal, and from dimensional arguments the dissipation rate can be related to the integral scale i.e. $\epsilon \propto U^3/\Lambda$. By substitution it can be shown that $t_\Lambda/\tau_\eta \propto Re_\Lambda^{1/2}$. This scaling was used for the new production term for Re_Λ.

The appropriate scaling for Re_υ was more challenging to determine. The first assumption made was that production must grow inversely proportional to Re_υ. This seems a logical assumption; that is, integral scales feed energy into the production mechanisms and at scales proportional to Kolmorogov's velocity scale energy is removed. To determine the exponent used for Re_υ in equation 6, the fundamental relationship for the growth of TKE presented in [23] was invoked i.e. LKE grows as $\sqrt{k_L} = \sqrt{k_{L_\infty}}(\omega_d x/U_\infty)$. Hinze [37] shows that the driving frequency can be approximated as $\omega_d \approx 0.1U_\infty/(\nu^3/\epsilon_\infty)^{1/4}$. By substitution, and making the assumption that $\epsilon_\infty \propto k_{L_\infty}$ (see equation 10), it can be shown that the growth of LKE is proportional to $k_{L_\infty}^{3/4}$. This result allowed for a first approximation. The approach followed in this work was to make the growth of LKE $\propto k_L^{3/4}$, taking into account the main production term $k_L S$ and Re_υ (which includes a factor of 1/4, see equation 7). Therefore, to have a total proportionality of 3/4, the contribution of the Kolmorov-based Reynolds number should be $\propto Re_\upsilon^{-1}$. However, it was found that the growth of LKE was overpredicted when using this approximation. As a result, the final form used was $\propto Re_\upsilon^{-13/10}$.

Additionally, as part of the proposed LKE model a new diffusion model due to wall-normal velocity fluctuations is proposed as shown in equation 4, where the effects of wall-normal fluctuations is included via a laminar diffusion "eddy" viscosity, α_L.

$$-\frac{\partial}{\partial y}\left(\overline{v'}k_L - \nu\frac{\partial k_L}{\partial y}\right) \approx \frac{\partial}{\partial y}\left[\left(\sigma_{k_L}\alpha_L + \nu\right)\frac{\partial k_L}{\partial y}\right] \tag{4}$$

Here, it is assumed that an additional diffusion mechanism is present towards the edge of the boundary layer due to the interaction of wall-normal fluctuations, $\overline{v'}$ and the LKE, k_L. The entire diffusion term derived in [23] (equation 1) is modelled using an "effective viscosity" approach similar to many turbulence models (equation 4). However, it was found that this new diffusion mechanism could not be model in a way analogous to that used in turbulence models, where the turbulent eddy viscosity is incorporated into the diffusion term. Instead, a new laminar "diffusion" eddy viscosity is defined as $\sqrt{k_L}y$. The laminar diffusion model assumes that wall-normal velocity fluctuations, v', are $\mathcal{O}(\sqrt{k_L})$. Also, the value of v' is small near walls, therefore, multiplication by the wall distance, y, not only helps provide dimensional consistency but it also limits the effect of this term near walls (where k_L is usually small). Finally, the new LKE model extracts momentum from the mean flow using the same used in eddy viscosity turbulence model. The laminar "eddy" viscosity, ν_L, is used to estimate the Reynolds stresses which in turn appear in the RANS momentum equation. This process is briefly presented in section 2.5. All model equations a presented in the next section.

2.3. Model equations

The general transport equation for the new model is shown in equation 5. The model involves three transport mechanisms: production, dissipation and diffusion (first, second and third terms on the right-hand side).

$$\frac{Dk_L}{Dt} = P_{k_L} - \epsilon + \frac{\partial}{\partial x_j}\left[\left(\nu + \sigma_{k_L}\alpha_L\right)\frac{\partial k_L}{\partial x_j}\right] \tag{5}$$

A new production term is proposed and shown in equation 6. It uses the classic strain-based approach. However, there is a linear relationship between the mean strain rate and production of LKE. Contrary to turbulence models which often define production in terms of the eddy viscosity, ν_t, and S^2.

$$P_{k_L} = \eta k_L S\left(Re_\upsilon^{-13/10}\right)\left(Re_\Lambda^{1/2}\right) \tag{6}$$

The production of LKE is scaled in terms of a dissipation Reynolds number (at the Kolmogorov scale), Re_υ, and an integral scale Reynolds number, Re_Λ, which are defined in equations 7 and 8, respectively:

$$Re_\upsilon = \frac{\upsilon y}{\nu} = \frac{(\epsilon\nu)^{1/4}y}{\nu} = \frac{\left(\frac{2\nu^2 k_L}{y^2}\right)^{1/4}y}{\nu} \tag{7}$$

$$Re_\Lambda = \frac{\|U_i\|y}{\nu} \tag{8}$$

The production coefficient η takes the functional form shown in equation 9.

$$\eta(Tu_{eff}) \approx c_1\tanh(c_2 Tu_{eff}^{c_3} + c_4); \tag{9}$$

It scales the growth of LKE based on an "effective" turbulence intensity, Tu_{eff}. For the geometries investigated in this work, Tu_{eff} is approximated using the value of the freestream turbulence intensity near the leading edge. The procedure to determine this function is detailed in section 2.6. The values given to the various coefficients are summarised in table 1. The near wall dissipation of LKE takes the familiar form shown in equation 10.

$$\epsilon = \frac{2\nu k_L}{y^2} \tag{10}$$

A new laminar diffusion "eddy" viscosity model is used to capture diffusion due to wall-normal velocity fluctuations and is defined as shown in equation 11.

$$\alpha_L = \sqrt{k_L}y \tag{11}$$

Finally, a "laminar eddy viscosity" is defined as shown in equation 12.

$$\nu_L = \frac{P_{k_L}}{\max\left\{S^2, \left(\frac{\|U_i\|}{y}\right)^2\right\}} \tag{12}$$

This is analogous to the definition of the production term used in many eddy viscosity models i.e. $P_k = \nu_t S^2$. The limit is used to ensure that in regions of low mean strain rate (e.g. the freestream) equation 12 is not divided by zero (or near zero) which would lead to unrealistically large values of ν_L. The laminar "eddy" viscosity is then fed into the RANS equations via the Boussinesq approximation (equation 16 - this process is described in more detail in section 2.5).

2.4. Boundary conditions and configuration

At wall boundaries, due to the no slip condition, the velocity components are equal to zero. Therefore, the appropriate boundary condition for k_L is also zero. At flow inlets, since k_L represents the energy of the velocity fluctuations in the streamwise direction only, it is calculated using equation 13. This definition is different to that of the turbulent kinetic energy used by models that assume isotropic turbulence, which estimate it as $k = 3/2(U_\infty Tu_\infty)^2$.

$$k_{L_{inlet}} = \frac{1}{2}\left(U_{inlet} Tu_{eff}\right)^2 \tag{13}$$

Where, Tu_{eff} is conceptually defined as the turbulence level that drives the initial freestream flow perturbations into the boundary layer. From a practical point-of-view, the value of the freestream turbulence intensity close to the leading edge (or object) may be chosen.

2.5. Implementation in OpenFOAM

The model equations presented in section 2.3 were implemented in OpenFOAM 4.x. This software has been chosen due to the relative ease and flexibility it offers to facilitate the implementation of new models. It is developed by the OpenFOAM Foundation and OpenCFD (trade mark owner). Since users have access to the source code, OpenFOAM has been gaining popularity in academia and its validity for scientific research has been established (e.g. [38]).

The new model is implemented within the RANS framework. The continuity and momentum equations for an incompressible fluid are shown in equation 14 and 15, respectively.

$$\frac{\partial U_i}{\partial x_i} = 0 \tag{14}$$

$$U_i \frac{\partial U_j}{\partial x_j} = \frac{1}{\rho}\frac{\partial P}{\partial x_i} + \frac{\partial}{\partial x_j}\left(\nu \frac{\partial U_i}{\partial x_j} - \overline{u_i' u_j'}\right) \tag{15}$$

The Boussinesq approximation, as shown in equation 16, provides a means to incorporate the effect of pretransitional fluctuations (modelled as the laminar kinetic energy) on the mean flow. Here, the "laminar eddy viscosity" (equation 12) replaces the eddy viscosity used in many classic turbulence models:

$$-\overline{u_i' u_j'} = 2\nu_L S_{ij} - \frac{1}{3}\overline{u_k' u_k'}\delta_{ij} \tag{16}$$

The new model is implemented using the relatively new template class available since OpenFOAM 3.0. The advantage of this class is that the model is implemented only once and both an incompressible and compressible version of the model are generated when the source code is compiled. As an observation for those readers interested in implementing similar models in OpenFOAM, it is important to ensure that the internal function to correct the eddy viscosity is fully implemented to ensure that the turbulent thermal diffusivity is computed correctly by compressible solvers. Once the model is compiled it is accessible to both steady-state and transient solvers that employ the SIMPLE [39] or PISO [40] algorithms respectively. These algorithms essentially solve equations 14 and 15. Closure of the system of equations is achieved using the Boussinesq hypothesis (equation 16) which requires solving equation 5 to estimate ν_L. Following the solution of the transport equation for k_L, the entire field is bounded to ensure that any negative results are removed from the solution. This is the default solution procedure used in openFOAM for models that use the SIMPLE or PISO algorithms. As a note for the practical application of the LKE model, it was found that the solution remained positive and bounding by solver was not active, at least, for the simulations and configurations tested in this work.

2.6. Calibration

The new LKE model defines two coefficients that need to be calibrated. The first coefficient, η, appears on the production term (equation 6) and the second coefficient, σ_{k_L}, scales the contribution of diffusion due to pretransitional laminar fluctuations (appearing on the last term of equation 5). These coefficients were estimated using the results from ECOFTAC for the zero gradient flat plate dataset cases T3A–, T3A and T3B [36], corresponding to freestream turbulence intensity levels of 0.9%, 3% and 6%.

It was found that the diffusion coefficient, σ_{k_L}, has a weak dependence on the freestream turbulence level (decreasing as Tu_∞ increases), and for simplicity, it has been assumed to be constant. On the other hand, the production coefficient, η, increases non-linearly with the freestream (effective) turbulence level near the leading edge (see section 4.3 for definition of Tu_{eff}). Therefore, the coefficient η has been defined as a function, $\eta(Tu_{eff})$, of the effective freestream turbulence intensity (Tu_{eff}) as shown in equation 9. The coefficients used in the definition of $\eta(Tu_{eff})$ were determined by best-fit (over 95% confidence) choosing the values of η (see figure 2) that best captured the growth of the maximum streamwise velocity fluctuations for the T3A–, T3A and T3B test cases [36] (available on ERCOFTAC's website). A fourth point for $Tu_{eff} = 0$ was also included, such as $\eta(0) = 0$. Conceptually, the additional point ($\eta(0) = 0$) is justified as the theoretical case when $Tu_\infty = 0$. It is assumed that in the absence of any upstream disturbances there is no growth (amplification) of laminar fluctuations. This assumption allows the definition of $\eta(Tu)$ for cases were the effective freestream turbulence intensity is lower than 0.9%.

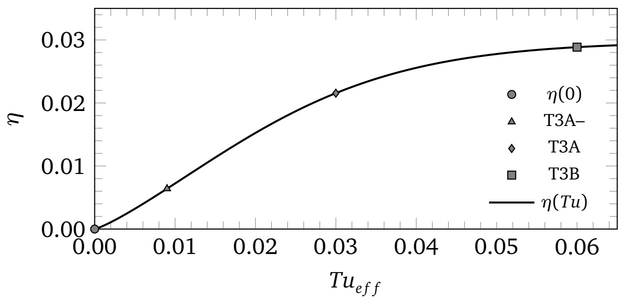

Figure 2: Proposed function for the production coefficient (solid line). Markers represent calibrated values corresponding to the T3A–, T3A and T3B ERCOFTAC ZPG flat plate cases [36]

Table 1: Summary of model coefficients

Coefficient	Value
σ_{k_L}	0.0125
C_1	0.02974
C_2	59.79
C_3	1.191
C_4	1.65×10^{-13}

It must be stressed that the new LKE model has only been strictly calibrated for freestream turbulence intensities in the range $0.009 \leq Tu \leq 0.06$. The calibration range is suitable for many internal flow applications (e.g. turbo-machinery [41], automotive emission systems [42], etc.) or external flows with moderate freestream turbulence (e.g. wind turbines [43]).The model coefficients used in this work are shown in table 1. Details about the test cases and the numerical set up used to carry out the model calibration are presented in more detail in section 3.1.

3. LKE model validation

3.1. Pre-transitional velocity fluctuations and skin friction

The simulations were carried out on a computational domain consisting of two blocks (figure 3) discretised using a structured hexahedral mesh. A grid independence study was also performed to ensure the effect of the grid on the solution is negligible (less than 1% change on the average skin friction over the plate and the average velocity over a profile sampled at $1.45m$ from the start of the plate). The grid used had 30x86x1 cells in the first block and 550x86x1 in the second block (in the x, y and z-directions), giving a total of 49,880 cells. The corresponding maximum y^+ value for the selected grid was 1.23 and the average y^+ value was 0.16 (for the case T3A– case which has the highest freestream velocity). A steady state incompressible flow solver (simpleFoam) based on the SIMPLE algorithm [39] was used to perform the calculations. Convergence of the simulations was assumed when the residuals for all variables dropped below 10^{-6}.

In regards to the discretisation of the model equations, in OpenFOAM end-users have the freedom to select discretisation schemes for each term that appears in the set of equations to be solved. In the simulations presented in this work

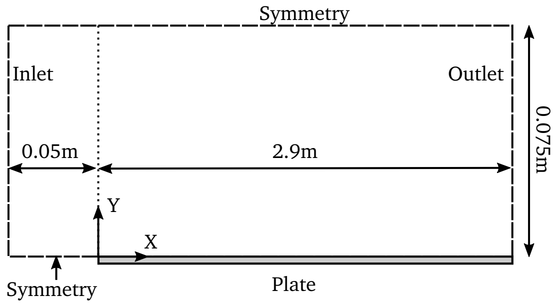

Figure 3: Schematic of the domain for the simulations of a flat plate at ZPG

Table 2: Summary of test conditions. EROFTAC ZPG test cases [36]

Case	Tu_{eff} [-]	U_∞ $[m/s]$	k_L $[m^2/s^2]$	ν $[m^2/s]$
T3A–	0.9%	19.3	0.0150	1.515×10^{-5}
T3A	3.0%	5.4	0.0115	1.497×10^{-5}
T3B	6.0%	9.4	0.1524	1.521×10^{-5}

the various terms in the model equations were discretised using the standard finite volume discretisation of Gaussian integration. The gradient terms require the interpolation of values between cell centres to face centres which was achieved using linear interpolation. For Laplacian terms, diffusion coefficients were discretised using linear interpolation. Surface normal gradients were discretised using a corrected scheme which offers second order accuracy. Finally, divergence terms were evaluated using a blended linear upwind scheme offering first/second order accuracy. This scheme was selected because it provides a suitable compromise between stability and accuracy.

The boundary just upstream of the plate and the top boundary are given a symmetry condition. At the plate, the pressure is prescribed as a Neumann boundary. At the outlet the velocity is prescribed as a Neumann boundary and the pressure is set up as a Dirichlet boundary with a nominal pressure of zero pascals. At the inlet, the pressure is set up as a Neumann boundary. The velocity is prescribed as a Dirichlet boundary. The LKE is defined as discussed in section 2.4.

To calibrate the model, a nominal inlet velocity of 10 m/s (with $\nu = 1.5 \times 10^{-5}$ m^2/s) is arbitrarily chosen. The coefficient η is adjusted to match the growth of the maximum non-dimensional streamwise velocity fluctuations for the the T3A–, T3A and T3B ERCOFTAC test cases, which correspond to Tu_∞ values of 0.9%, 3% and 6%. Assuming $Tu_\infty \approx Tu_{eff}$, individual η coefficients for each case (shown in figure 2) are used to develop the functional form of the production coefficient $\eta(Tu_{eff})$ that was shown in equation 9. The validity of this function is checked using the experimental results of Dyban and Epik [44], for which $Tu_\infty = 1.6\%$, representing a different value of Tu_{eff} compared to those used during calibration (i.e. not 0.9%, 3% or 6%). Since for this case $Tu_\infty \approx Tu_{eff} = 1.6\%$, it falls comfortably between the 0.9% and 3% turbulence intensity ERCOFTAC test cases. Figure 4 shows that the new LKE model predictions agree well with

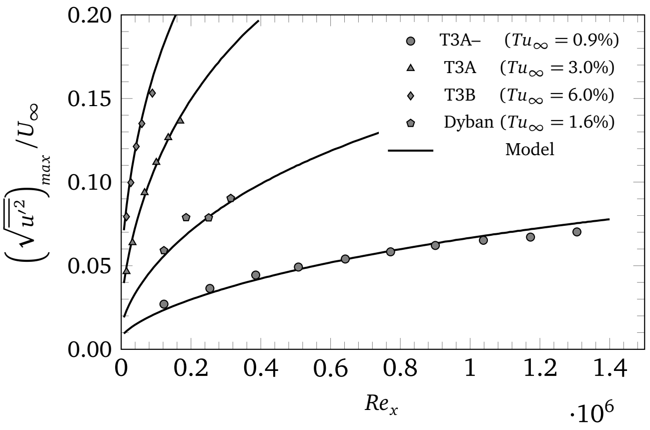

Figure 4: Maximum streamwise velocity fluctuations. The model was calibrated using the T3A–, T3A and T3B cases [36]. Results by Dyban [44] demonstrate predictive capability

the Dyban and Epik's [44] case. Figure 4 also shows that the agreement between the new model and the ERCOFTAC experiments is excellent. These results combined provide confidence on the validity of the proposed function $\eta(Tu_{eff})$.

To ensure that the model's predictions of laminar fluctuations scale appropriately, three additional simulations are performed based on the ERCOFTAC T3A–, T3A and T3B cases. The simulations are based on the same grid and numerical set up used for the calibration cases. However, the inlet conditions are defined to match the experiments. A summary of the inlet conditions for these simulations is shown in table 2. These simulations are performed in order to confirm that the model correctly predicts the development of streamwise pretransitional velocity fluctuations regardless of the magnitude of the inlet velocity i.e. their growth depends only on the relative scale of the inflow fluctuations (Tu).

Figure 5 presents profiles of the wall normal distribution of the root-mean-square of streamwise velocity fluctuations at various stations along the plate (given as the local Reynolds number, Re_x). These figures show that, overall, the proposed model's predictions are in good agreement with experimental results. For the T3A– case ($Tu = 0.9\%$), the model underpredicts the growth of $\sqrt{\overline{u'^2}}$ at $Re = 2.541 \times 10^5$ and $Re = 6.422 \times 10^5$ and overpredicts it for the T3A and T3B cases. However, the agreement is quite remarkable considering the relative simplicity of the new model.

The new model defines a laminar "eddy" viscosity, ν_L (equation 12), which is used as part of the Boussinesq approximation (equation 16) and it enters the momentum equation (equation 15) via the Reynolds stress tensor. Thus, and analogous to RANS turbulence models, the effect of laminar velocity fluctuations is to extract momentum from the mean flow and this is achieved using ν_L. The model also defines a new laminar diffusion "eddy" viscosity, α_L (equation 11), which has been designed to enhance the diffusion of k_L due to velocity fluctuations near the boundary layer edge. Figure 6 shows typical profiles of k_L, ν_L, α_L at $Re_x = 1.443 \times 10^6$ for the T3A case . For comparison, the Blasius velocity profile

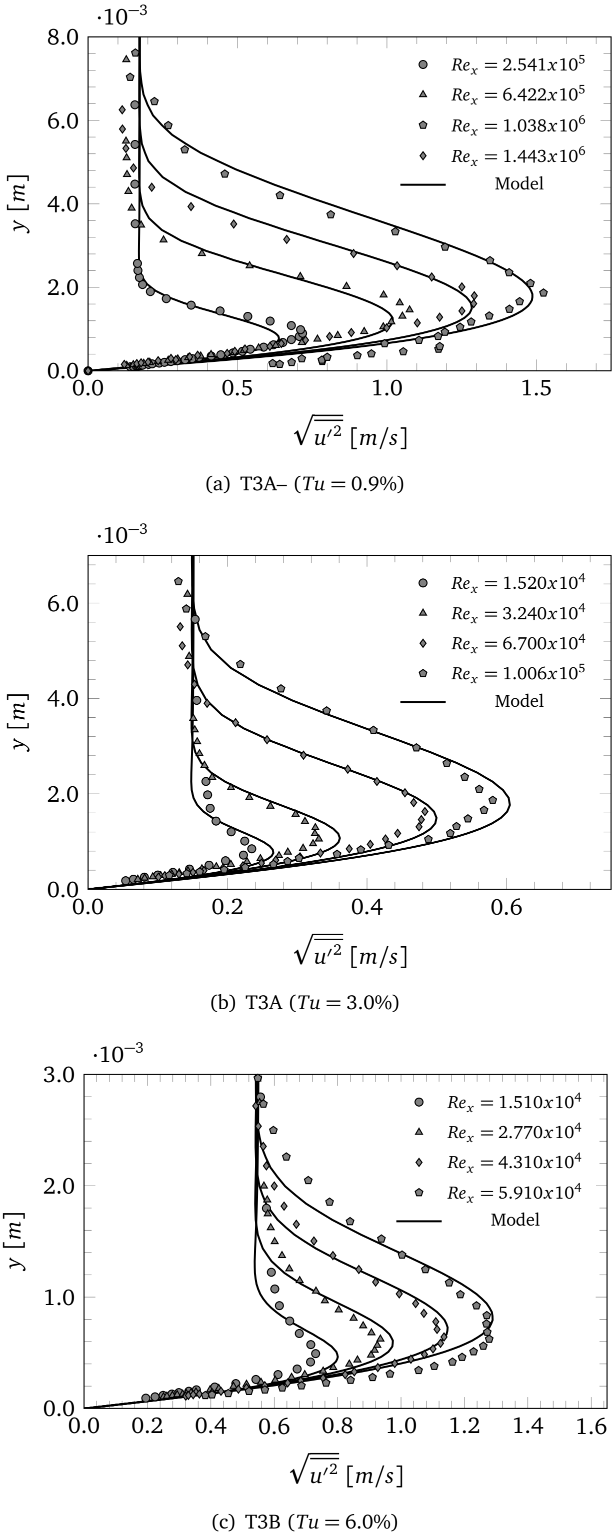

Figure 5: Streamwise velocity fluctuations profiles predicted at various local Reynolds numbers for the ERCOFTAC ZPG test cases. Markers correspond to measurements [36]

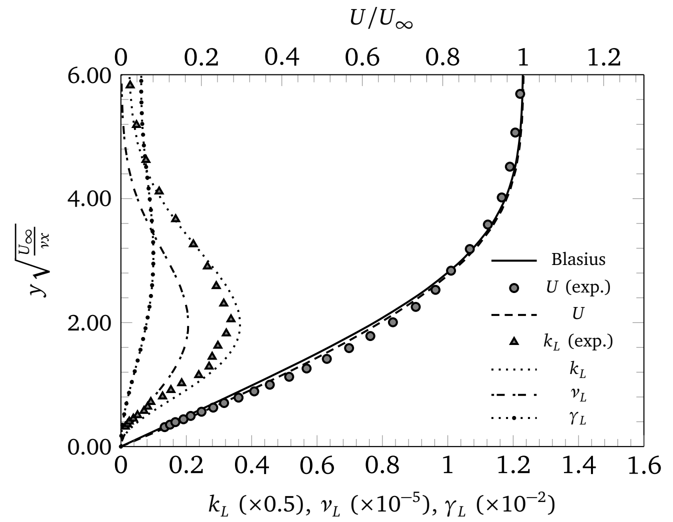

Figure 6: Typical profiles for several variables of interest. Scaling shown in brackets. Symbols and units are defined in the nomenclature. Top axis scale used for the velocity (U) only

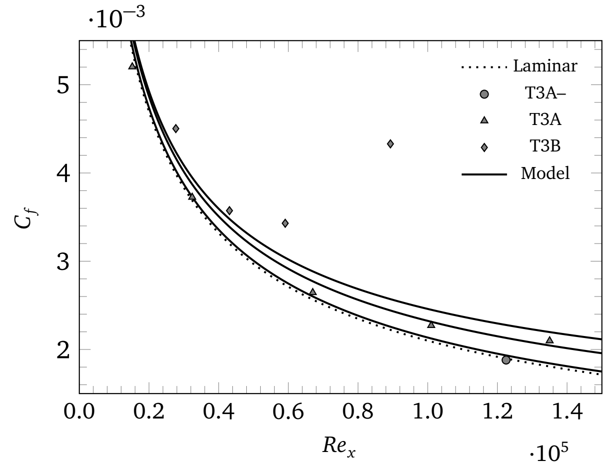

Figure 7: Model predictions for the skin friction distribution along the plate at different freestream turbulence intensities. Markers present experimental results [36] for comparison

and the predicted velocity profile are also included. There is generally good agreement with the experiment. The maximum LKE is overpredicted by approximately 8%. The predicted velocity profile marginally deviates from the Blasius solution. However, the experimental velocity profile deviates from the Blasius solution by a maximum of approximately 15% at $y\sqrt{U_\infty/\nu x} \approx 1.75$. This suggests that the new model underpredicts ν_L and, consequently, its effect on the mean flow is not pronounced. This is an ideal feature to simplify the incorporation of the new LKE model into existing turbulence models. Considering that the profiles plotted in figure 6 correspond to a local Reynolds number of $Re_x = 1.443 \times 10^6$, this location is close to the critical Reynolds number for the T3A case. Therefore, it could be suggested that this deviation from the laminar velocity profile could be modelled by coupling the new LKE with a turbulence model and using an intermittency-type blending function between models (e.g. [45]).

As the freestream turbulence level is increased, the velocity profiles predicted by the new model exhibit a small deviation from the laminar velocity profile. This is due to the influence of ν_L on the mean flow. In order to assess the effect that these changes have on the predicted skin friction coefficient, its distribution along the plate for the ERCOFTAC ZPG test cases will be evaluated. The skin friction coefficient definition is given in equation 17:

$$C_f = \frac{\tau_w}{\frac{1}{2}\rho U_\infty^2} \tag{17}$$

Figure 7 shows that there is a very good agreement between the model's predictions and the experimental results. In all the test cases, the model predicts values of the skin friction coefficient that initially follow the laminar theoretical solution [31] and, as the local Reynolds number is increased (i.e. moving away from the leading edge of the plate), the predicted skin friction coefficient increases and deviates from the laminar theoretical solution. This trend is more pronounced as the freestream turbulence intensity increases which indicates that the freestream turbulence intensity level influences the mean velocity profile in the pretransitional boundary layer and results in an increase in the local skin friction coefficient. Whilst this observation is not new [46, 47], figure 7 shows that the new LKE model is capable of capturing this behaviour. This is an encouraging result since it points to the possibility that the model proposed in this work could be utilised to complement existing turbulence models to develop new transition sensitive models. This is a task for which the current model is particularly suitable since it does not rely on auxiliary variables e.g. such as the dependence of k_L on k and ω in the formulation of the $k - k_L - \omega$ model [22].

4. Coupling the new LKE model with a turbulence model

4.1. Background

The new LKE model has been shown to be capable of predicting pretransitional velocity fluctuations along a flat plate with remarkable accuracy given its relatively simple formulation. From a practical point-of-view, this LKE model offers the possibility to complement existing turbulence models to enable them to predict boundary layer transition. In fact, Mayle and Shulz [7] and Walters et al. [20–22] have already established that the laminar kinetic energy concept can be used to predict boundary layer transition. However, their respective approaches for developing transitional models cannot be readily generalised as discussed earlier. Therefore, a more flexible method to couple the new LKE model with existing turbulence models is desirable. The ideal approach would require no modifications to the new LKE model and only minor modifications to the chosen turbulence model. In this section, a method to couple the new LKE model with

Wilcox's $k-\omega$ model [28] is presented. The resulting 3-equation transition model will be referred to as the $k-\omega$ LKE model (to use a name that clearly differentiates the model from the $k-k_L-\omega$ [22]). The ultimate objective is to illustrate the potential of the new LKE to predict boundary layer transition within a coupling framework that is both relatively simple and flexible.

There are a number of possible methods that can be used to couple the new LKE model with a turbulence model. For example, Walters et al. [20–22] use an energy transfer method in which the pre-transitional LKE is converted into turbulent kinetic energy. In this work, this method will not be adopted due to its complexity (which originates from the need to incorporate a number of auxiliary functions), and due to the fact that this method inherently requires to modify the background LKE model. Intermittency-based approaches that employ a separate transport equation (e.g. [48]) are not desirable since they would result in increased computational costs and will not be explored here. Therefore, an algebraic-type method is preferred.

Kubacki and Dick [29, 30] present a simple approach to convert a standard $k-\omega$ turbulence model into a transition model that requires only minimal modifications to the baseline turbulence model. Overall, their approach relies on the inclusion of an algebraic "starting" or "trigger" function into the production term of the turbulent kinetic energy equation. To couple the new LKE model with the $k-\omega$ model an approach inspired on their work will be adopted.

In [29], a number of parameters or relationships that can be (and have been) used to develop "starting" functions are presented. These are presented in equations 18, 19 and 20. For succinctness, a detailed discussion of their physical interpretation is not included here and the reader is referred to the work of Kubacki and Dick [29].

$$Re_y = \frac{\sqrt{k}y}{\nu} \tag{18}$$

$$Re_\omega = \frac{k\omega}{\nu\Omega^2} \tag{19}$$

$$Re_\Omega = \frac{k}{\nu\Omega} \tag{20}$$

Kubacki and Dick [29] stress that any of these expressions can be used as transition onset parameters. Walters and Cokljat [22] used the onset parameters defined by equations 18 and 20. Buckaki et al. [29, 30, 49] have used all three relationships. However, in [30], they concluded that the onset parameter described in equation 18 offered the best predictions of transition onset location. They argue that near the wall, the streamwise velocity fluctuations, u', in a pre-transitional boundary layer are caused by streaks and assume that they scale with $y\Omega$. Additionally, they suggest that $\sqrt{k}$ can be used to represent near-wall normal velocity fluctuations, v'. Therefore, the turbulent shear stress near the wall, $-\rho u'v' \propto \rho y\Omega\sqrt{k}$. Wang et al. [50] noted that breakdown to turbulence occurs when the ratio of the turbulent shear stress to the wall shear stress reaches a critical value. The wall shear stress is $\tau_w = \rho\nu\Omega_{wall}$. Therefore, Kubacki and Dick [30] conclude that $Re_y = \sqrt{k}y/\Omega$ can be used as a suitable onset parameter. In this work, however, since a model for the pretransitional velocity fluctuations is available, the turbulent shear stress near the wall can be assumed to be proportional to the LKE i.e. $-\rho u'v' \propto \rho k_L$. Here, the ratio between turbulent shear stress and the wall shear stress can be represented as shown in equation 21 and it will be used as the onset parameter:

$$Re_\Omega = \frac{k_L}{\nu\Omega} \tag{21}$$

In the next section, details of a transitional $k-\omega$ model are presented. The coupling approach used to develop the new $k-\omega$ LKE model is based largely on the work of Kubacki and Dick [29, 30]. However, the $k-\omega$ LKE model uses a new onset parameter and "trigger" functions. Additionally, the predictions over the transition and turbulent regions are improved by including the "trigger" function into the diffusion terms of the transport equations for k and ω, so that their diffusion within laminar regions is only affected by the molecular viscosity.

4.2. Transitional $k-\omega$ LKE model equations

The transitional $k-\omega$ LKE is a 3-equation model. Transport equations are solved for the turbulent kinetic energy (equation 22), the specific dissipation rate (equation 23) and the laminar kinetic energy (equation 5):

$$\frac{Dk}{Dt} = \gamma f_\nu P_k - \gamma C_\mu k\omega + \frac{\partial}{\partial x_j}\left[\left(\nu + \sigma_k\gamma\frac{k}{\omega}\right)\frac{\partial k_L}{\partial x_j}\right] \tag{22}$$

$$\begin{aligned}\frac{D\omega}{Dt} &= C_{\omega 1}P_k\frac{\omega}{k} - C_{\omega 2}\omega^2 + \frac{\partial}{\partial x_j}\left[\left(\nu + \sigma_\omega\gamma\frac{k}{\omega}\right)\frac{\partial k_L}{\partial x_j}\right] \\ &\quad + \frac{\sigma_d}{\omega}\frac{\partial k}{\partial x_j}\frac{\partial \omega}{\partial x_j}\end{aligned} \tag{23}$$

The production of turbulent kinetic energy is modelled using the classical stress-strain approach as the product between the Reynolds stress tensor, τ_{ij}, and the mean velocity gradient as shown in equation 24:

$$P_k = \tau_{ij}\frac{\partial U_i}{\partial x_j} \tag{24}$$

The Reynolds stress tensor is modelled using a linear eddy viscosity formulation based on the Boussinesq approximation as shown in equation 25:

$$\tau_{ij} = \nu_t\left(2S_{ij} - \frac{2}{3}\frac{\partial U_k}{\partial x_k}\delta_{ij}\right) - \frac{2}{3}k\delta_{ij} \tag{25}$$

Similar to the approach of Walters et al. [20–22] and Kubacki and Dick [29, 30], in the proposed $k-\omega$ LKE model, the total eddy viscosity is separated into a small and a large scale eddy viscosity. The small scale eddy viscosity, $\nu_{t,s}$, is defined as:

$$\nu_{t,s} = f_{SS}\frac{k}{\omega} \tag{26}$$

A shear-sheltering function [22] is used to remove low frequencies from the turbulent kinetic energy [29] and is defined as:

$$f_{SS} = e^{-(C_{SS}/Re_{SS})^2} \tag{27}$$

Where the shear-sheltering Reynolds number is defined as:

$$Re_{SS} = \frac{k}{\nu\Omega} \tag{28}$$

A viscous damping function [22] is used to control the production of turbulent kinetic energy near walls (equations 29 and 30):

$$f_\nu = 1 - e^{\sqrt{Re_T}/C_\nu} \tag{29}$$

$$Re_T = \frac{k}{\nu\omega} \tag{30}$$

The viscous damping function ensures that the production of turbulent kinetic energy becomes zero at walls and it facilitates the use of wall-resolving grids.

The transition onset parameter introduced in section 4.1 is implemented as shown in equation 31:

$$Re_L = \frac{k_L}{\min(\nu, \nu_L)\Omega} \tag{31}$$

The limit is imposed to allow an increase of the value of the onset parameter in the turbulent boundary layer. In turn, it allows the "trigger" function to reach a value of unity closer to wall boundaries such that the production of turbulent kinetic energy corresponds closely to that of the fully turbulent model. This enables the model to return improved predictions of the skin friction distribution within turbulent regions, in contrast to the formulation used by Kubacki and Dick [29, 30], which tends to underpredict the fully turbulent skin friction coefficient. The trigger function is defined as:

$$\gamma = \frac{\min\left(Re_L^2, C_{crit}\right)}{C_{crit}} \tag{32}$$

Finally, the eddy viscosity is calculated by adding the effects of small and large scale fluctuations (equation 33):

$$\nu_t = \nu_{t,s} + \nu_L \tag{33}$$

Where, the small scale viscosity, $\nu_{t,s}$, is calculated using equation 26 and the large scale eddy viscosity contribution is computed from the laminar eddy viscosity, ν_L, obtained from the LKE model (equation 12).

4.3. Boundary conditions and configuration

The transitional $k-\omega$ LKE model requires a grid that resolves the boundary layer down to the viscous sub-layer. Therefore, it is recommended that the first grid point is located at $y^+ \approx 1$. At wall boundaries, since the velocity is zero, the turbulent kinetic energy, k, is also zero. The specific dissipation rate, ω, uses the classic solution for smooth walls shown in equation 34.

$$\omega_{wall} = \frac{6\nu}{C_{\omega 2}y^2} \tag{34}$$

The wall and inlet conditions for the laminar kinetic energy should be prescribed as described in section 2.4.

4.4. Model calibration and implementation

The model was calibrated against the ERCOFTAC zero-pressure gradient flat plate test cases (T3A–, T3A and T3C) [36], allowing to tune the model to various freestream turbulence levels. To ensure an appropriate response of the model to freestream conditions, the inlet conditions are chosen to replicate the turbulence decay recorded during the experiments (see section 5.1). Only three coefficients require calibration. The coefficients C_{SS} and C_ν were calibrated using the T3A case. These coefficients adopt the highest value possible such that further increases result in a deviation of the turbulent skin friction coefficient from the theoretical distribution. The coefficient C_{crit} controls the predicted location of transition onset and is tuned to provide the best possible agreement with the experiments for all the test cases. The remaining coefficients adopt the default values of the original turbulence model [28]. A summary of the closure coefficients is provided in table 3.

The model is implemented in OpenFOAM following essentially the same procedure as described in section 2.5. However, in addition to solving the transport equation for k_L (equation 5), the transport equations for k (equation 22) and ω (equation 23) are also included in the solution process. Finally, the Reynolds stress tensor is estimated using the Boussinesq approximation (equation 25).

5. Transitional $k-\omega$ LKE model validation

The purpose of this section is to establish the validity and usefulness of the new LKE model to be used in conjunction

Table 3: Summary of coefficients for the $k-\omega$ LKE model

Coefficient	Value
C_μ	0.09
$C_{\omega 1}$	0.52
$C_{\omega 2}$	0.0708
C_{crit}	76,500
C_{SS}	1.45
C_v	0.43
σ_k	0.50
σ_d	0.125
σ_ω	0.50

with a turbulence model for the prediction of transitional flows. Following the coupling approach detailed above results in a 3 equation RANS model ($k-\omega$ LKE) that should be capable of predicting transition onset. The performance of the transitional $k-\omega$ LKE model is benchmarked using three configurations: (i) a flat plate at a zero pressure gradient, (ii) a variable pressure gradient flat plate and (iii) a laminar separation bubble. The performance of the $k-\omega$ LKE model is assessed by comparison with both experimental results and the predictions from the $k-k_L-\omega$ model [22] (a well-known and popular transition model which also uses the LKE concept for the prediction of transitional flows).

5.1. Flat plate at a zero pressure gradient

The $k-\omega$ LKE model is first tested on a flat plate at zero pressure gradient. The simulations were set up to match the ERCOFTAC experiments for a plat plate at zero pressure gradient for three different freestream turbulence levels (table 2). A schematic of the computational domain is shown figure 8. The domain was comprised of two blocks which were discretised using a structured hexahedral mesh. Following a grid convergence assessment, the first block which covered the region of the domain upstream of the flat plate was discretised with 30x86x1 cells. The block used to discretised the region of the domain representing the flat plate had 700x86x1 cells. The total number of cells was 62,780. The grid spacing in the y-direction was chosen to ensure that $y^+ \approx 1$. The maximum value of y^+ was 1.28 for the T3A– case. The transport equations were discretised as described in section 3.1. However, limiters were employed for calculating the gradients used to approximate the divergence terms in the k, ω and k_L equations. The system of equations was solved using the SIMPLE [39] algorithm. The boundary conditions for the velocity and pressure fields are prescribed as detailed in section 3.1, with the exception of the top boundary which is configured as a slip boundary. The boundary conditions for k_L are described as detailed in section 2.4, for k and ω they are specified as indicated in section 4.3. The inlet conditions for k and ω are chosen to replicate the freestream turbulence decay recorded during the experiments as shown in figure 9. A summary of the inlet conditions used is presented in table 4.

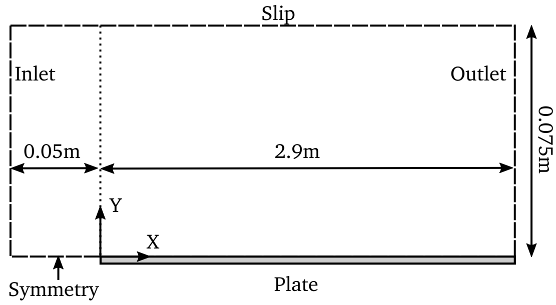

Figure 8: Schematic of the domain for the simulations of a flat plate with ZPG

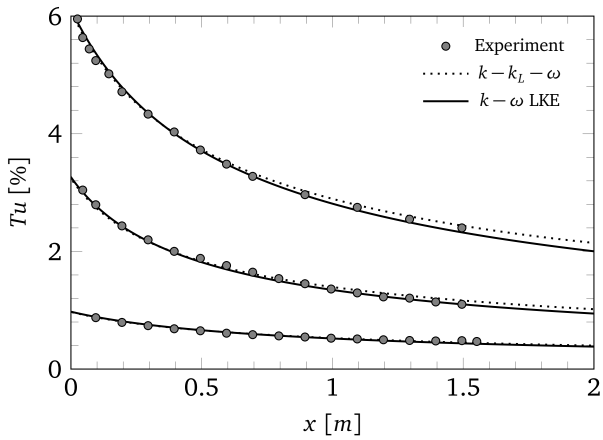

Figure 9: Turbulence decay for the T3A-, T3A and T3B cases.

The predicted skin friction coefficient distributions for the T3A–, T3A and T3B test cases is presented in figure 10. For comparison, the experimental measurements and the predictions from the $k-k_L-\omega$ model [22] are also included. For the T3A– case, the transition onset is marginally underestimated compared with the experiment. For the T3A case, the agreement is excellent. However, for the highest (6%) freestream turbulence intensity test case (T3B), the model overpredicts the distribution of the skin friction coefficient along the laminar boundary. This behaviour is attributed to the inability of either the viscous damping function or the "trigger" function to limit the production of turbulent kinetic energy in the laminar region at higher turbulence intensity levels. To address this behaviour additional damping of k is required which could be achieved by introducing other function(s) to further control the production of k, or by modifying the ω equation. However, this would increase the complexity of the model and requires further investigation. Nonetheless, the results demonstrate that the new LKE model can be used to develop new transition models. The coupled $k-\omega$ LKE model can predict the onset of transition with remarkable accuracy for the flat plate test cases, especially when considering the relative simplicity of the model.

5.2. Flat plate with a variable pressure gradient

The ERCOFTAC database also offers the T3C series of experimental results for a flat plate with variable pressure gra-

Table 4: Summary of test conditions for the test cases for a flat plate at zero-pressure gradient.

Case	Model	Tu_{eff} [-]	U_{inlet} $[m/s]$	k $[m^2/s^2]$	k_L $[m^2/s^2]$	ω $[s^{-1}]$	ν_R [-]
T3A-	$k-k_l-\omega$	-	19.3	0.0595	10^{-15}	49	7.3
	$k-\omega$ LKE	0.009	19.3	0.0595	0.0151	507	7.8
T3A	$k-k_l-\omega$	-	5.4	0.0575	10^{-15}	27	12.7
	$k-\omega$ LKE	0.03	5.4	0.0575	0.0115	275	13.9
T3B	$k-k_l-\omega$	-	9.4	0.5850	10^{-15}	35.3	99.6
	$k-\omega$ LKE	0.06	9.4	0.5850	0.1524	365	106.8

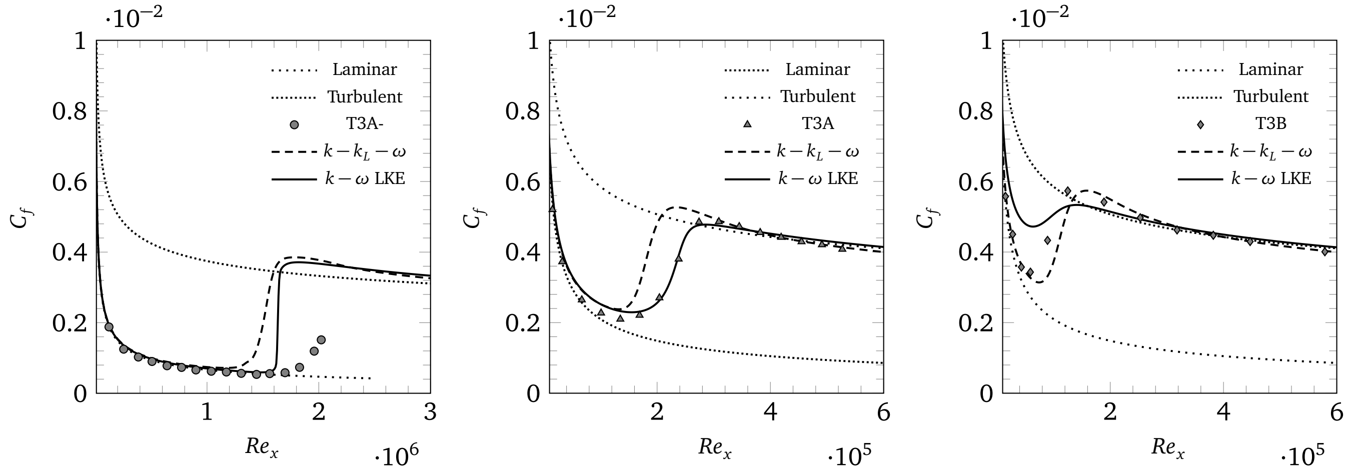

(a) T3A- ($Tu = 0.9\%$) (b) T3A ($Tu = 3.0\%$) (c) T3B ($Tu = 6.0\%$)

Figure 10: Streamwise skin friction coefficient distributions for the ERCOFTAC ZPG test cases [36]

dient [36]. The pressure gradient is imposed by varying the profile of the wind tunnel's top wall. The transition onset location is adjusted by increasing or decreasing the wind tunnel's freestream velocity. For a similar freestream turbulence intensity level (approx 2.5%), transition occurs over regions where the pressure gradient is favourable (T3C5), adverse (T3C3) or corresponds to the suction peak (T3C2). These varying pressure test cases are included to demonstrate that the formulation of both the LKE and the $k{-}\omega$ LKE models can also be used for more challenging configurations. The simulations demonstrate that the models response is appropriate for both adverse and favourable pressure gradients.

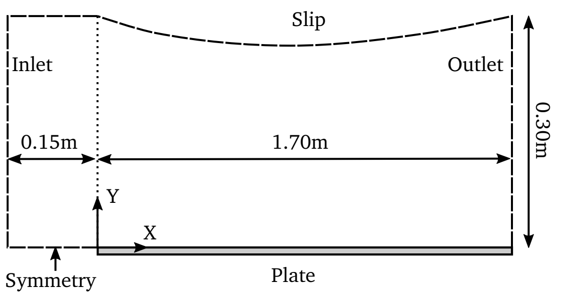

Figure 11: Schematic of the domain for the simulations of a flat plate with imposed pressure gradient

The simulations were performed using a computational domain with a varying top boundary profile as illustrated in figure 11. The top boundary profile is used to match the freestream velocity along the place measured during the experiments and it was defined using the polynomial expression previously employed by Suluksna et al. [51]. Following a grid independence study, the domain was discretised with hexahedral cells using two blocks. The first block containing 50x72x1 cells and the second block (covering the plate) comprised 1000x72x1 cells for a total of 75,600 cells. The maximum y^+ was approximately 1.5 (T3C5 case). The model equations were solved and discretised using the same numerical procedure and schemes described in section 5.1. The boundary conditions were configured as described in section 5.1 (see also sections 2.4 and 4.3). The turbulent kinetic energy and the specific dissipation rate were defined at the inlet to reproduce the experimental decay of the turbulence intensity for each case as shown in figure 12. The inlet velocity was chosen so that the resulting velocity field matched the experimental velocity distribution along the flat plate (figure 12). For convenience, a summary of the inlet conditions is presented in table 5.

In figure 13, the predicted streamwise skin friction coefficient distributions are compared with the experiments. Overall, the agreement between the experiments and the predicted skin friction is excellent. The $k-\omega$ LKE model is able

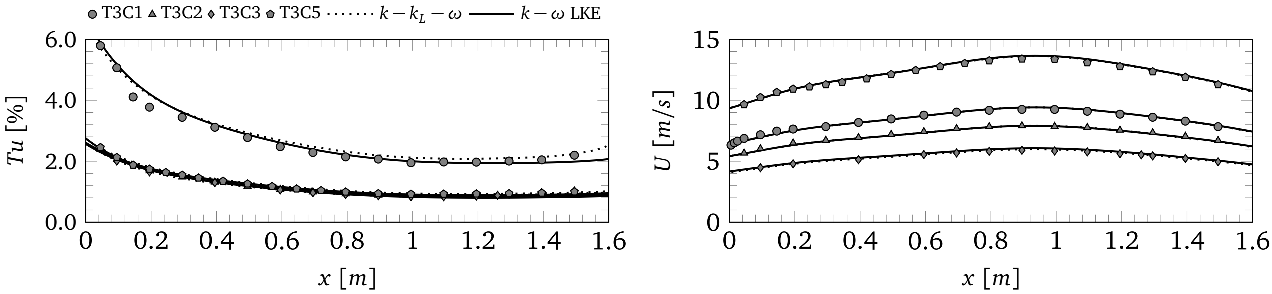

(a) Turbulence decay

(b) Velocity distribution

Figure 12: Turbulence decay and velocity distribution for the T3C1, T3C2, T3C3 and T3C5 cases.

Table 5: Summary of test conditions for the T3C variable pressure gradient test cases.

Case	Model	Tu_{eff} [-]	U_{inlet} [m/s]	k [m^2/s^2]	k_L [m^2/s^2]	ω [s^{-1}]	ν_R [-]
T3C1	$k-k_l-\omega$	-	6.05	0.791	10^{-15}	80	59.3
	$k-\omega$ LKE	0.077	6.05	0.791	0.109	742	72.8
T3C2	$k-k_l-\omega$	-	5.1	0.068	10^{-15}	44	9.3
	$k-\omega$ LKE	0.025	5.1	0.068	0.007	380	11.9
T3C3	$k-k_l-\omega$	-	3.80	0.054	10^{-15}	54	6.0
	$k-\omega$ LKE	0.025	3.80	0.048	0.014	445	7.2
T3C5	$k-k_l-\omega$	-	8.80	0.235	10^{-15}	82	17.2
	$k-\omega$ LKE	0.025	8.80	0.170	0.023	565	20.0

to predict a transition onset location close to that given by the experiments. For the T3C3 case (adverse pressure gradient), the model overestimates the location of the transition onset by approximately 6%. With the exception of the T3C3 case, the model estimates transition onset more accurately than the $k-k_L-\omega$ model which overestimates it for all cases. This finding is surprising since the $k-k_L-\omega$ model is shown to perform reasonably well for the T3C2, T3C3 and T3C5 cases by Walters and Cokljat [22]. The difference in performance may be due to the fact that their domain includes a semi-circular leading edge. Here, a fully sharp leading edge is used to represent of the experimental setup. This suggests that the choice to represent the leading edge geometry affects the predictions and requires further investigation to be able to define and promote precise best-practice guidelines for the usage and application of transitional models in general.

5.3. Laminar separation bubble

In order to test the robustness of the new LKE model and the $k-\omega$ LKE model, as well as to assess their potential applicability to more complex configurations, a laminar separation bubble (LSB) test case is presented in this section. Since the LKE model has been designed specifically to operate under the conditions encountered in by-pass transition, its application to a LSB configuration should yield results comparable to a laminar solution, albeit with a marginal transfer of momentum from the mean flow to the mean fluctuating velocity in the streamwise direction due to the influence of the "laminar eddy viscosity" defined in equation 12.

The numerical set up used is the same as that detailed in section 3.1. The case was solved using a transient solver available in OpenFOAM (pimpleFoam) which can operate as a hybrid between the PISO and SIMPLE algorithms. In this case, it was configured to operate in PISO mode. Temporal derivatives were calculated using the implicit second-order accurate backward scheme. The convergence criteria between time steps was 10^{-6} for the pressure and 10^{-5} for all other variables. The solver automatically adjusts the time step in order to maintain the maximum Courant number below a user-defined value; here set to 1. The simulations ran for a total of 1.5 seconds and the results presented in this section correspond to the time-averaged solution for the time interval from 0.5 seconds to 1.5 seconds. The first 0.5 seconds of simulated time are disregarded in order to allow the simulation to settle.

The computational domain used is shown in figure 14. It was discretised using a structured hexahedral mesh consisting of two blocks with a total of 53,009 cells. A grid independence study was conducted following a similar approach as described in the previous sections. However, for this case the average calculated from pressure distribution along the flat plate was used as reference. The corresponding maximum y^+ value for the selected grid was 1.67 and the average y^+ value was 0.54.

At the inlet, the values of the velocity vector and the LKE (again, estimated using equation 13), k and ω are prescribed whilst the pressure is assigned a zero gradient boundary condition. At the outlet, a pressure outlet boundary is prescribed

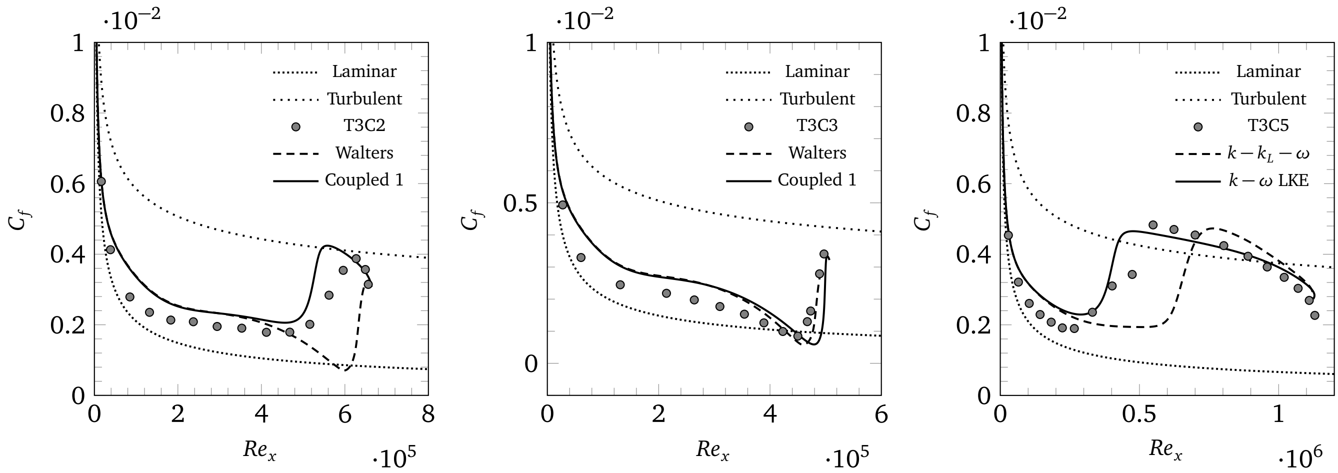

(a) T3C2 ($Tu = 3.0\%$) (b) T3C3 ($Tu = 6.0\%$) (c) T3C5 ($Tu = 6.0\%$)

Figure 13: Streamwise skin friction coefficient distributions for the ERCOFTAC variable pressure gradient test cases [36]

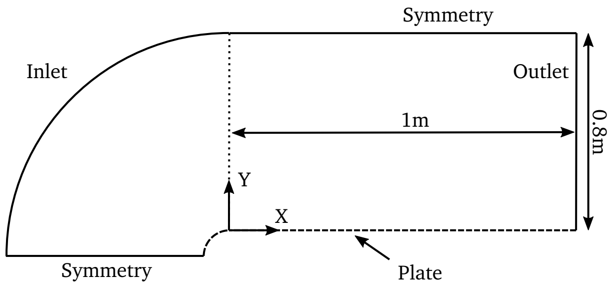

(a) Schematic of the computational domain

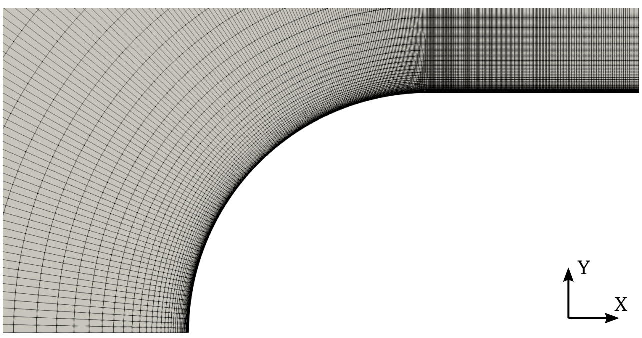

(b) Mesh close up

Figure 14: Domain schematic and close up of the grid used (leading edge)

and the gradient for all other variables leaving the computational domain is set to zero. A symmetry condition is assigned to the top boundary and the boundary just upstream of the plate. At the plate, the pressure is defined as a Neumann boundary, a no-slip condition is used for the velocity vector and the laminar kinetic energy is zero. The laminar "eddy" viscosity is also set to zero at the wall (following its definition in equation 12).

In order to gain a broad understanding of the performance of the new models, the laminar separation bubble experimental configuration and results presented by Samson and Sarkar [52] are used for comparison. Additionally, to provide as broad a picture as possible of their predictions, results are compared against solutions provided from laminar, transitional and turbulent models. The laminar solution is obtained using a dummy turbulence model which sets the eddy viscosity (therefore, the Reynolds stresses) equal to zero in the momentum equation (equation 15). The transitional results are obtained using the transitional $k - k_L - \omega$ model [22]. The fully turbulent solution is generated using the popular k–ω SST RANS model [53]. Table 6 provides a summary of the test conditions for the simulations carried out.

Figure 15 shows time-averaged pressure coefficients profiles along the plate. The definition of the pressure coefficient, as used by Samson et al. [52], is given in equation 35.

$$C_p' = \frac{C_p - C_{p_{min}}}{C_{p_{max}} - C_{p_{min}}} \tag{35}$$

In this work, simulations were carried out to correspond with the lowest and highest values of the Reynolds number reported by Samson et al. [52] and are equal to $Re = 25,000$ and $Re = 75,000$.

Although, Samson et al. [52] also reported velocity profiles at various stations along the separation bubble, due to

Table 6: Summary of test conditions for the laminar separation bubble test cases.

Case	Model	Re [-]	Tu_{eff} [-]	U_{inlet} $[m/s]$	k $[m^2/s^2]$	k_L $[m^2/s^2]$	ω $[s^{-1}]$	ν_R [-]
LSB1	Laminar	25×10^3	-	4.68	-	-	-	-
LSB2	Laminar	75×10^3	-	14.0	-	-	-	-
LSB3	$k-k_l-\omega$	25×10^3	-	4.68	1.38×10^{-3}	10^{-15}	8.35	1
LSB4	$k-k_l-\omega$	75×10^3	-	14.0	1.24×10^{-2}	10^{-15}	75.2	1
LSB5	$k-\omega$ SST	25×10^3	-	4.68	1.38×10^{-3}	-	92.8	1
LSB7	$k-\omega$ SST	75×10^3	-	14.0	1.24×10^{-2}	-	835.4	1
LSB8	LKE	25×10^3	0.0065	4.68	-	4.63×10^{-4}	-	-
LSB6	LKE	75×10^3	0.0065	14.0	-	4.17×10^{-3}	-	-
LSB9	$k-\omega$ LKE	25×10^3	0.0065	4.68	1.38×10^{-3}	4.63×10^{-4}	92.5	1
LSB10	$k-\omega$ LKE	75×10^3	0.0065	14.0	1.24×10^{-2}	4.17×10^{-3}	828	1

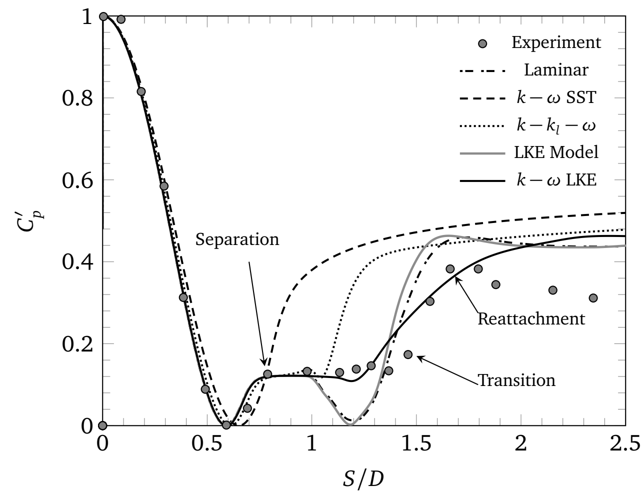

(a) $Re = 25,000$

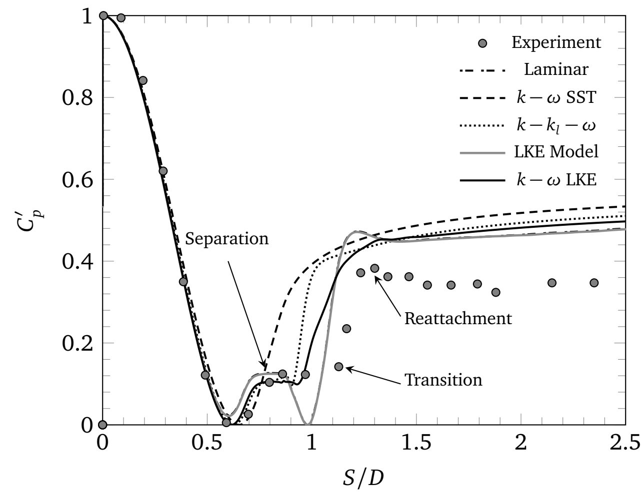

(b) $Re = 75,000$

Figure 15: Time-averaged pressure distribution coefficient along the plate. Markers represent measurements [54]

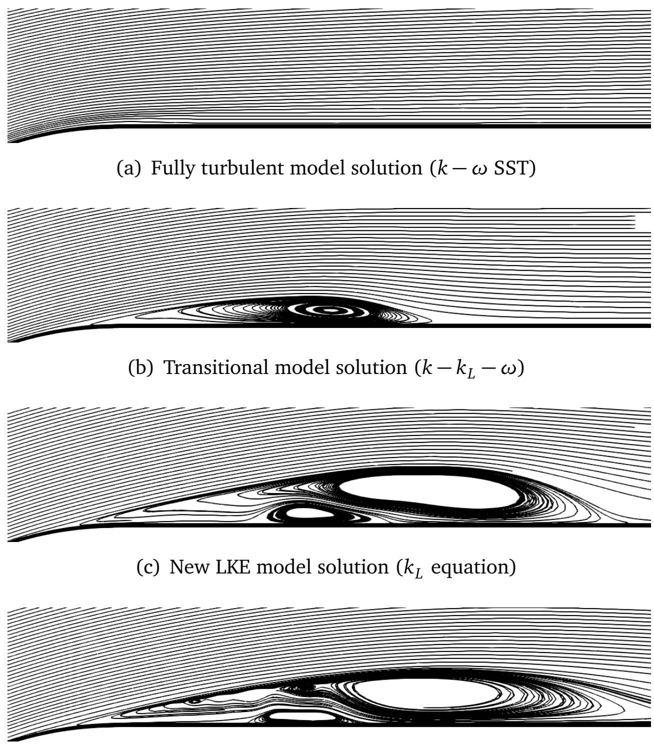

(a) Fully turbulent model solution ($k-\omega$ SST)

(b) Transitional model solution ($k-k_L-\omega$)

(c) New LKE model solution (k_L equation)

(d) Coupled transitional model solution ($k-\omega$ LKE)

Figure 16: Streamlines calculated from the time-averaged velocity for various models tested at $Re = 25,000$

limitations inherent to the experimental technique used (hot-wire anemometry), such as its inability to provide reliable measurements in areas of reversed flow, only pressure measurements are used for comparison herein. Nonetheless, this does not impair the general assessment of the new models. To facilitate the interpretation of results, the procedure proposed by Gerakpulos et al. [55] to identify the onset of separation, transition and reattachment is used. These regions of interests are labelled accordingly in figures 15(a) and 15(b). Following a local pressure minimum at $S/D \approx 0.6$, there is a region exhibiting a pressure plateau which has been attributed to the onset of separation [56, 57]. The end of reattachment corresponds to the peak in the adverse pressure gradient region and the onset of transition is estimated as the intersection of the best fit lines through the pressure plateau and the adverse pressure gradient region [52].

Figure 15 shows that regardless of the Reynolds number tested the fully turbulent model ($k-\omega$ SST [53]) completely fails to capture the main features of the laminar separation bubble. The $k-k_L-\omega$ model [22] captures the general features of the laminar separation bubble. However, the laminar separation bubble transitions and reattaches in a length roughly half of that of the experiments. Although it is difficult to conclusively identify the reason for the reduction in the predicted length of the laminar separation bubble, it is possible that the tendency of the $k-k_L-\omega$ model to overpredict the laminar kinetic energy (e.g. figure 1) can result in an unintended energy drain from the mean flow. Accordi and de Lemos [45] also identified this weakness of the $k-k_L-\omega$ model and proposed damping function to reduce the production of LKE away from the wall in pretransitional regions and despite their modification the model's weakness to capture separation induced transition was still present. The new LKE model underpredicts the length of the laminar separation bubble by approximately 20% and 15% for $Re = 25,000$ and $Re = 75,000$ respectively. The location of the reattachment region is underpredicted by approximately 10%. The new model also predicts an unphysical secondary pressure reduction within the pressure plateau, similar to the prediction of the laminar model. The presence of this secondary pressure drop is attributed to the formation of a strong recirculation bubble which originates as a result of a lack of energy transfer from the mean flow into turbulence. This means that the momentum in the outer region of the separation bubble is not lost in the process of sustaining turbulence, and as the flow turns onto itself a strong vortex forms (from examination of streamlines - see figure 16) which in turn leads to a reduction in the local pressure. This result is not surprising since the new LKE model does not include a means to account for the generation of turbulence. In fact, figure 15 shows that the LKE model does indeed return essentially the laminar solution and the difference between the results from the laminar and the new LKE model is negligible. In contrast, the $k-\omega$ LKE model has the ability to generate turbulence and allow the required loss of momentum towards the edge of the separation bubble. This results in a drastic improvement of the pressure distribution predictions. Figure 15 shows that for both cases, the $k-\omega$ LKE can capture the major physical features, particularly for $Re = 25,000$. This result is particularly encouraging since it shows the potential for the model to be used in applications involving laminar separation bubbles which can be particularly challenging to study numerically.

6. Conclusion

A new model for the laminar kinetic energy (LKE) has been proposed and validated. To the authors' knowledge only two frameworks to model the LKE exist. The approach by Mayle and Schulz [23] is elegant but has some practical limitations. For example, information about the freestream turbulence spectrum is required. This information is not always available. The approach by Walters et al. [20–22] is pioneering and it was the first to highlight the potential of employing the LKE to develop general purpose transition-sensitive models. However, it was found that their most well-know model [22] fails to accurately predict the magnitude of the LKE for turbulence intensities below 6%.

In the process of developing the new LKE model, it was shown that the production of LKE can be modelled using the classic strain-based approach and it can be scaled with functions to represent the integral length scale and Kolmogorov velocity scale Reynolds numbers. To the authors' knowledge, for the first time a model is presented to account for the diffusion due to the interaction of wall-normal velocity fluctuations and the LKE. This was achieved through a laminar diffusion "eddy" viscosity. The model was validated against the zero pressure gradient flat plate ECOFTAC test cases. Despite the relative simplicity of the new model, its predictions of the velocity fluctuations and LKE are in excellent agreement with the experiments. Furthermore, an approach is illustrated that allows to couple the LKE model with a version of Wilcox's $k-\omega$ model and results in a new 3-equation transition model ($k-\omega$ LKE model).

The $k-\omega$ LKE model was validated using a number of test cases involving transitional flows. The agreement between predictions and experiments was excellent for all the configurations tested, including the transitional flow other a flat plate, a flat plate with variable pressure gradient and a laminar separation bubble. Although further testing of this model is required to fully understand its limitations, the results presented in this work are very promising considering the relative simplicity of both the coupling method and the resulting model.

References

[1] Y. S. Kachanov, Physical mechanisms of laminar-boundary-layer transition, Annual Review of Fluid Mechanics 26 (1) (1994) 411–482. doi:10.1146/annurev.fl.26.010194.002211.

[2] W. Saric, H. Reed, E. Kerschen, Boundary-layer receptivity to freestream disturbances, Annual Review of Fluid Mechanics 34 (2002) 291–319. doi:10.1146/annurev.fluid.34.082701.161921.

[3] A. M. O. Smith, N. Gamberoni, Transition, pressure gradient and stability theory, Report ES 26388, Douglas Aircraft Company (1956).

[4] A. M. O. Smith, Transition, pressure gradient and stability theory, in: Proceedings of the 9th International Conference of Applied Mechanics, Vol. 4, 1956, pp. 234–244.

[5] J. L. van Ingen, A suggested semi-empirical method for the calculation of the boundary layer transition region, in: Proceedings of the Second European Aeronautical Congress, 1956, pp. 37.1 – 37.16.

[6] B. Abu-Ghannam, R. Shaw, Natural transition of boundary layers - the effects of turbulence, pressure gradient, and flow history, Journal of Mechanical Engineering Science 22 (5) (1980) 213–228.

[7] R. E. Mayle, Role of laminar-turbulent transition in gas turbine engines, ASME journal of turbomachinery 113 (4) (1991) 509–537.

[8] L. Chen, X. Liu, M. Oliveira, C. Liu, Dns for late stage structure of flow transition on a flat-plate boundary layer, in: 48th AIAA Aerospace Sciences Meeting Including the New Horizons Forum and Aerospace Exposition, 2010.

[9] V. Borodulin, V. Gaponenko, Y. Kachanov, D. Meyer, U. Rist, Q. Lian, C. Lee, Late-stage transitional boundary-layer structures. direct numerical simulation and experiment, Theoretical and Computational Fluid Dynamics 15 (5) (2002) 317–337. doi:10.1007/s001620100054.

[10] T. André, A. Durant, I. Fedioun, Numerical study of supersonic boundary-layer transition due to sonic wall injection, AIAA Journal 55 (5) (2017) 1530–1547. doi:10.2514/1.J055164.

[11] S. Makino, M. Inagaki, M. Nakagawa, Laminar-turbulence transition over the rotor disk in an enclosed rotor-stator cavity, Flow, Turbulence and Combustion 95 (2-3) (2015) 399–413. doi:10.1007/s10494-015-9619-z.

[12] V. Mistry, G. Page, J. McGuirk, Simulation of receptivity and induced transition from discrete roughness elements, Flow, Turbulence and Combustion 95 (2-3) (2015) 301–334. doi:10.1007/s10494-015-9636-y.

[13] H. Choi, P. Moin, Grid-point requirements for large eddy simulation: Chapman's estimates revisited, Physics of Fluids 24 (1). doi:10.1063/1.3676783.

[14] D. C. Wilcox, Turbulence Modeling for CFD, 3rd Edition, DCW Industries, 2006.

[15] Y. Suzen, P. Huang, Modeling of flow transition using an intermittency transport equation, Journal of Fluids Engineering, Transactions of the ASME 122 (2) (2000) 273–284.

[16] J. Steelant, E. Dick, Modeling of laminar-turbulent transition for high freestream turbulence, Journal of Fluids Engineering, Transactions of the ASME 123 (1) (2001) 22–30.

[17] F. Menter, R. Langtry, S. Likki, Y. Suzen, P. Huang, S. Völker, A correlation-based transition model using local variables part i - model formulation, in: Proceedings of the ASME Turbo Expo 2004, Vol. 4, 2004, pp. 57–67.

[18] F. Menter, P. Smirnov, T. Liu, R. Avancha, A one-equation local correlation-based transition model, Flow, Turbulence and Combustion 95 (4) (2015) 583–619. doi:10.1007/s10494-015-9622-4.

[19] J. Edwards, C. Roy, F. Blottner, H. Hassan, Development of a one-equation transition/turbulence model, AIAA Journal 39 (9) (2001) 1691–1698. doi:10.2514/2.1526.

[20] D. Walters, J. Leylek, A new model for boundary layer transition using a single-point rans approach, Journal of Turbomachinery 126 (1) (2004) 193–202. doi:10.1115/1.1622709.

[21] D. Walters, J. Leylek, Computational fluid dynamics study of wake-induced transition on a compressor-like flat plate, Journal of Turbomachinery 127 (1) (2005) 52–63. doi:10.1115/1.1791650.

[22] D. Walters, D. Cokljat, A three-equation eddy-viscosity model for reynolds-averaged navier-stokes simulations of transitional flow, Journal of Fluids Engineering, Transactions of the ASME 130 (12) (2008) 1214011–12140114. doi:10.1115/1.2979230.

[23] R. Mayle, A. Schulz, The path to predicting bypass transition, Journal of Turbomachinery 119 (3) (1997) 405–411.

[24] H. Medina, J. Early, Modelling transition due to backward-facing steps using the laminar kinetic energy concept, European Journal of Mechanics, B/Fluids 44 (2014) 60–68. doi:10.1016/j.euromechflu.2013.10.004.

[25] Y. Qin, C. Yan, Z. Hao, L. Zhou, A laminar kinetic energy transition model appropriate for hypersonic flow heat transfer, International Journal of Heat and Mass Transfer 107 (2017) 1054 – 1064. doi:https://doi.org/10.1016/j.ijheatmasstransfer.2016.11.012.

[26] V. Chitta, D. K. Walters, Prediction of aerodynamic characteristics of an elliptic airfoil at low reynolds number, in: ASME Paper No. FEDSM2012-72389, 2012.

[27] Y. Zhang, Z. Sun, A. van Zuijlen, G. van Bussel, Numerical simulation of transitional flow on a wind turbine airfoil with rans-based transition model, Journal of Turbulence (2017) 1–20doi:10.1080/14685248.2017.1334908.

[28] D. Wilcox, Formulation of the k-ÏL' turbulence model revisited, AIAA Journal 46 (11) (2008) 2823–2838. doi:10.2514/1.36541.

[29] S. Kubacki, E. Dick, An algebraic model for bypass transition in turbomachinery boundary layer flows, International Journal of Heat and Fluid Flow 58 (2016) 68 – 83. doi:https://doi.org/10.1016/j.ijheatfluidflow.2016.01.001.

[30] S. Kubacki, E. Dick, An algebraic intermittency model for bypass, separation-induced and wake-induced transition, International Journal of Heat and Fluid Flow 62 (2016) 344 – 361. doi:https://doi.org/10.1016/j.ijheatfluidflow.2016.09.013.

[31] H. Schlichting, K. Gersten, Boundary layer theory, 8th Edition, Springer-Verlag, 2000.

[32] P. S. Klebanoff, Effects of free-stream turbulence on a laminar boundary layer, Bulletin of the American Physical Society 16 (1971) 1323.

[33] C. C. Lin, Motion in the boundary layer with a rapidly oscillating external flow, in: Proceedings of the 9th International Congress of Applied Mechanics, Vol. 4, 1957, pp. 155–167.

[34] S. Lardeau, M. Leschziner, N. Li, Modelling bypass transition with low-Reynolds-number nonlinear eddy-viscosity closure, Flow, Turbulence and Combustion 73 (1) (2004) 49–76. doi:10.1023/B:APPL.0000044367.24861.b7.

[35] S. Lardeau, N. Li, M. Leschziner, Large eddy simulation of transitional boundary layers at high free-stream turbulence intensity and implications for RANS modeling, Journal of Turbomachinery 129 (2) (2007) 311–317. doi:10.1115/1.2436896.

[36] J. Coupland, T3a and t3b test cases, ERCOFTAC Special Interest Group.

[37] J. O. Hinze, Turbulence, 2nd Edition, New York, N.Y. : McGraw-Hill, 1975.

[38] E. Robertson, V. Choudhury, S. Bhushan, D. Walters, Validation of OpenFOAM numerical methods and turbulence models for incompressible bluff body flows, Computers and Fluids 123 (2015) 122–145. doi:10.1016/j.compfluid.2015.09.010.

[39] S. Patankar, D. Spalding, A calculation procedure for heat, mass and momentum transfer in three-dimensional parabolic flows, International Journal of Heat and Mass Transfer 15 (10) (1972) 1787–1806. doi:10.1016/0017-9310(72)90054-3.

[40] R. I. Issa, Solution of the implicitly discretised fluid flow equations by operator-splitting, Journal of Computational Physics 62 (1) (1986) 40 – 65.

[41] I. Shahin, M. Alqaradawi, M. Gadala, O. Badr, Large eddy simulation of surge inception and active surge control in a high speed centrifugal compressor with a vaned diffuser, Applied Mathematical Modelling 40 (23) (2016) 10404 – 10418. doi:https://doi.org/10.1016/j.apm.2016.07.030.

[42] S. Porter, J. Saul, S. Aleksandrova, H. Medina, S. Benjamin, Hybrid flow modelling approach applied to automotive catalysts, Applied Mathematical Modelling 40 (19) (2016) 8435 – 8445. doi:https://doi.org/10.1016/j.apm.2016.04.024.

[43] M. Ahmadi-Baloutaki, R. Carriveau, D. S.-K. Ting, Performance of a vertical axis wind turbine in grid generated turbulence, Sustainable Energy Technologies and Assessments 11 (Supplement C) (2015) 178 – 185. doi:https://doi.org/10.1016/j.seta.2014.12.007.

[44] E. P. Dyban, E. I. Epik, Heat and mass transfer and hydrodynamics of turbulent flows, Izdatel Naukova Dumka, 1985.

[45] I. Accordi, M. De Lemos, Single-point transition modeling using the laminar kinetic energy concept, International Journal of Heat and Mass Transfer 89 (2015) 1095–1109. doi:10.1016/j.ijheatmasstransfer.2015.05.040.

[46] D. Zhou, T. Wang, Effects of elevated free-stream turbulence on flow and thermal structures in transitional boundary layers, Transactions -

ASME: Journal of Turbomachinery 117 (3) (1995) 407–417.

[47] D. Zhou, T. Wang, Combined effects of elevated free-stream turbulence and streamwise acceleration on flow and thermal structures in transitional boundary layers, Experimental Thermal and Fluid Science 12 (3) (1996) 338–351. doi:10.1016/0894-1777(95)00125-5.

[48] F. Menter, R. Langtry, S. Likki, Y. Suzen, P. Huang, S. VÃűlker, A correlation-based transition model using local variables - part i: Model formulation, Journal of Turbomachinery 128 (3) (2006) 413–422. doi:10.1115/1.2184352.

[49] S. Kubacki, B. G. E. Dick, An algebraic intermittency model added to the $k-\omega$ RANS model for transition simulation, in: Proceedings of the 11th European Turbomachinery Conference, no. ETC2015-059, 2015.

[50] T. Wang, F. Keller, D. Zhou, Flow and thermal structures in a transitional boundary layer, Experimental Thermal and Fluid Science 12 (3) (1996) 352–363. doi:10.1016/0894-1777(95)00126-3.

[51] K. Suluksna, P. Dechaumphai, E. Juntasaro, Correlations for modeling transitional boundary layers under influences of freestream turbulence and pressure gradient, International Journal of Heat and Fluid Flow 30 (1) (2009) 66 – 75. doi:https://doi.org/10.1016/j.ijheatfluidflow.2008.09.004.

[52] A. Samson, S. Sarkar, An experimental investigation of a laminar separation bubble on the leading-edge of a modelled aerofoil for different reynolds numbers, Proceedings of the Institution of Mechanical Engineers, Part C: Journal of Mechanical Engineering Science 230 (13) (2016) 2208–2224. doi:10.1177/0954406215594826.

[53] F. R. Menter, M. Kuntz, R. Langtry, Ten years of industrial experience with the SST turbulence model, in: Proceedings of 4th International Symposium on Turbulence, Heat and Mass Transfer, no. 2010-4629, 2003, pp. 625–632.

[54] R. Schook, H. De Lange, A. Van Steenhoven, Heat transfer measurements in transitional boundary layers, International Journal of Heat and Mass Transfer 44 (5) (2001) 1019–1030. doi:10.1016/S0017-9310(00)00161-7.

[55] R. Gerakopulos, M. Boutilier, S. Yarusevych, Aerodynamic characterization of a naca 0018 airfoil at low reynolds numbers, in: Proceedings of the 40th AIAA Fluid Dynamics Conference, no. 2010-4629, 2010.

[56] N. Cherry, R. Hillier, M. Latour, Unsteady measurements in a separated and reattaching flow, Journal of Fluid Mechanics 144 (1984) 13–46. doi:10.1017/S002211208400149X.

[57] M. Brendel, T. Mueller, Boundary-layer measurements on an airfoil at low reynolds numbers, Journal of Aircraft 25 (7) (1988) 612–617. doi:10.2514/3.45631.